Performance Investigation of Two-, Three- and Four-Phase Bearingless Slice Motor Configurations

M.T. Bartholet*, S. Silber**, T. Nussbaumer***, J.W. Kolar*

* ETH Zurich, Power Electronic Systems Laboratory, 8092 Zurich, Switzerland, bartholet@lem.ee.ethz.ch
** LCM, Linz Center of Mechatronics GmbH, 4040 Linz, Austria
*** Levitronix GmbH, Technoparkstrass 1, 8005 Zurich, Switzerland

Abstract—**The fact that bearingless slice motors (BSM) are widely used in pump systems in the semiconductor industry and for medical applications has caused the attention of other industries for this emerging technology. Here, costs, power consumption and pump volume play an important role. Since the mechanical setup of the motor has a strong impact on these issues five different motor and converter setups are comparatively evaluated and discussed in this paper. The comparison will be carried out for two-, three- and four-phase BSM concepts based on performance indices such as power losses, power electronics requirements and cost-related realisation issues.**

I.   INTRODUCTION

In today's bearingless pump systems, which have successfully been launched on the market, a two-phase bearingless motor with a symmetrical configuration of the drive and bearing windings is used to actively control the impeller of the pump. This pump setup offers several advantages compared to conventional pumps currently employed in semiconductor and medical applications. The various benefits for the handling of ultra-pure and aggressive fluids in these markets are described in literature [1], [2].

Pharmaceutical, biotechnology and food processing applications are similar to the processes in the semiconductor industry in terms of purity requirements. They demand a high degree of sterility and precision to ensure the quality of the end product, eg. drugs, enzymes in biochemical processes or dairy, cereal and beverages in food processing applications. Standard centrifugal pumps cannot be used in these applications, since their ceramic housing does not sustain the hot steam, which is commonly used to sterilise the process plant. Therefore, mainly tube pumps are used in these applications. Although their maintenance costs are significantly higher compared to those of bearingless pumps their overall price is still lower than that of today's commercially available bearingless pump systems. Thus, if one manages to reduce the overall cost of a bearingless pump they can become very attractive for these markets.

Furthermore, a big potential for next generation bearingless pump systems is located in applications, where magnetically coupled pumps are currently used to deliver hazardous materials, e.g. chromic acid, sodium hypochlorite or sulphur dioxide. The biggest advantage of a bearingless pump compared to magnetically coupled pumps is the fact, that they can run dry without a destruction of their bearings and thus offer an extended lifetime in comparison to standard magnetically coupled pumps. Another very attractive area for more cost effective bearingless pump systems lies in the plating market. The problem with magnetically coupled pumps in that area is the fact that the plating material tends to be deposited in the narrow bearing gap which can result in a locking of the bearing. This problem especially arises in copper, gold and nickel

plating processes and often results in large down times of the production plant and maintenance costs of the pumps. Again, both factors can be significantly reduced with the use of a bearingless pump. Additional potential markets for BSM pumps with a strong demand for long durability without maintenance are heating and cooling pumps. An overview about the future application areas for bearingless pump systems is given in **Fig. 1**.

Recent research has mainly focused on the power electronics part of the system in order to decrease the complexity of the system and hence the manufacturing cost. As a result, new converter concepts featuring higher power density, higher efficiency and a lower number of power switches have been developed [3]. However, in order to attract the before described application areas the bearingless slice motor itself must be taken into account as well.

Due to the fact that the design of a BSM offers a lot of constructive freedom several different topologies have been developed over the last years [4]-[9]. They often highly differ in the way how the bearing forces and the motor torque are generated. Looking at the winding perspective, they can broadly be categorized into two groups. Namely, into those which comprise of a dual set of winding configurations [4]-[6] and a second group which only has a single set of winding configurations that carries both the torque and the levitation currents [7]-[9].

However, only one type has reached readiness for marketing in pump applications so far. Its temple motor design is depicted in **Fig. 2**. There it can be seen that the stabilisation of the impeller of the pump is realised with contactless magnetic bearings that are placed around the claws which are carrying the flux of the bearing and drive system. The six spatial degrees of freedom of the rotor are stabilised magnetically through the housing wall. This is done passively for
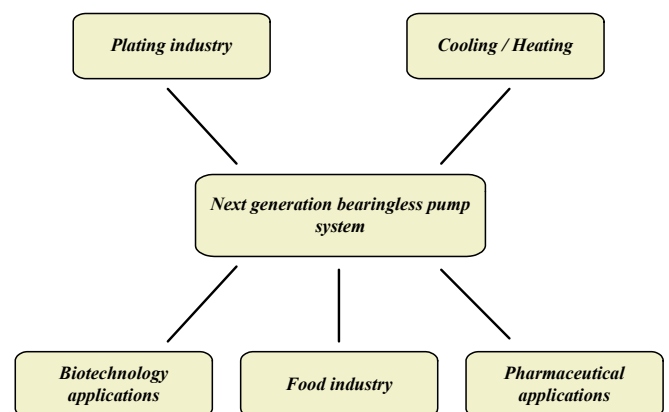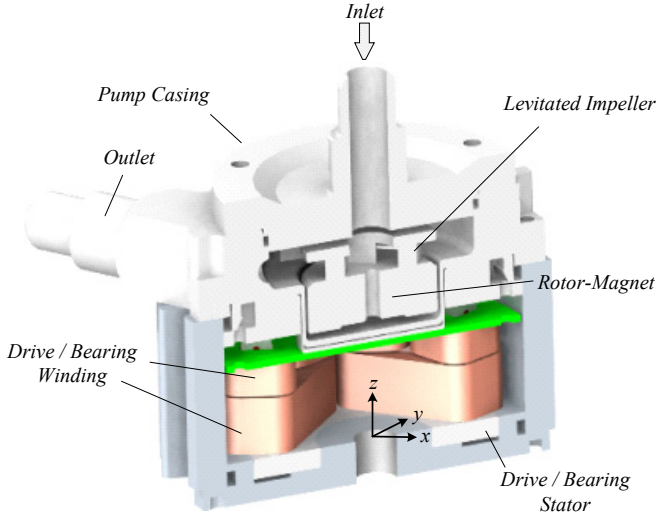

Fig. 1: Future application areas of next generation bearingless pump systems.

Fig. 2: Schematic of the basic principle of the bearingless centrifugal pump.

three of them, i.e. the axial displacement (in z-direction) and the angular displacement (tilting in x- and y-direction). The three remaining degrees of freedom are controlled actively, i.e. the radial displacement (in x- and y-direction) and the rotation of the rotor. Therefore, the active motor part generates the driving torque as well as the radial magnetic bearing forces. With this, an extremely compact design can be accomplished.

In order to achieve the before-mentioned complexity and cost reduction in this paper two-, three- and four-phase BSM configurations consisting of the motor and the power electronics are comparatively evaluated based on performance indices regarding volume, losses and cost with a strong focus on the suitability for future application. First, the force and torque model utilized to calculate the performance parameters is briefly presented in **section II**. Starting with the characteristics of the two-phase BSM with separated bearing and drive systems for torque and force generation, three-and four-phase motor configurations are then presented in **section III**. The comparison of these concepts is afterwards carried out in **section IV** where a detailed comparison of the copper, the iron and the power electronics losses is presented that occur in the different embodiments. Furthermore, in **section V** the necessary VA requirement needed to guarantee a safe operation of each motor is calculated. Finally, in **section VI**, cost-related realisation issues are discussed for the different concepts and the suitability of the presented assemblies for future applications of bearingless pump systems is evaluated.

II. FORCE AND TORQUE CALCULATION

The analytical force and torque model applied for the performance analysis of the hereafter discussed BSM configurations is explained in detail in [10]. Thus, only a brief summary of the theoretical fundamentals will be given here. The underlying simulations which provide the basis for the mathematical calculations of the losses and power requirements have been carried out with the electromagnetic field simulation program Maxwell [11] for all of the discussed motor embodiments.

With the precise knowledge of the electromagnetic field variables in the air gap a general force and torque model can be derived with the use of the Maxwell stress tensor $\boldsymbol{T}_M$ [12]

$$\boldsymbol{T}_M = \mu \begin{bmatrix} H_t^2 - \frac{1}{2}H^2 & H_t H_n & H_t H_z \\ H_n H_t & H_n^2 - \frac{1}{2}H^2 & H_n H_z \\ H_z H_t & H_z H_n & H_z^2 - \frac{1}{2}H^2 \end{bmatrix}. \quad (1)$$

Here, $\boldsymbol{H}$ is the magnetic field intensity, which is composed of

$$\boldsymbol{H} = \begin{bmatrix} H_t & H_n & H_z \end{bmatrix}^T, \ H = |\boldsymbol{H}|, \quad (2)$$

and μ is the permeability. The mechanical stress $\boldsymbol{\sigma}$ acting on a surface element can then be calculated with

$$\boldsymbol{\sigma} = \boldsymbol{T}_M \boldsymbol{e}_n, \quad (3)$$

where $\boldsymbol{e}_n$ represents the vector perpendicular to the stator surface (cf. **Fig. 3**). Furthermore, it is assumed that the permeability of the ferromagnetic stator is much higher than that of air and thus the tangential component of the flux density H_{1t} in the air gap can be neglected for the following calculation of the torque and the forces responsible for the levitation of the impeller.

With this, the mechanical tension $\boldsymbol{\sigma}_{12}$ on the interface between air (medium 1) and stator iron (medium 2) can be approximated by

$$\boldsymbol{\sigma}_{12} = \begin{bmatrix} \dfrac{B_{1n}^2}{2\mu_0} \\ B_{1n} J_s \\ 0 \end{bmatrix}, \quad (4)$$
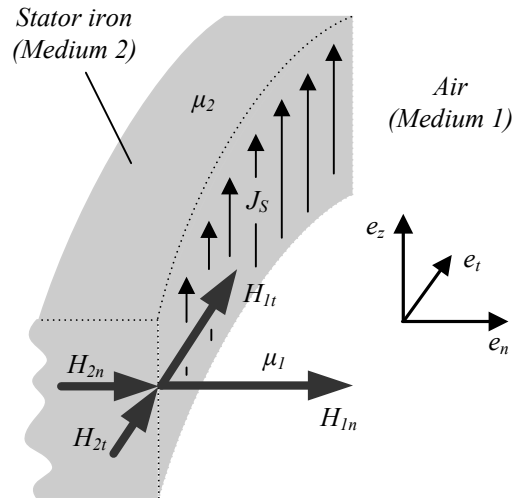
where J_s is the current density distribution on the stator surface, which is assumed of cylindrical shape, and B_{1n} is the normal component of the flux density in air.

The force and torque acting on the rotor of the BSM are then determined by the surface integral

$$F = \oint_A \sigma_{12} dA, \quad (5)$$

where A represents the area of the surface.

The currents in the drive and bearing systems which provide the basis for the comparison of the hereafter presented motor configurations are obtained with this mathematical model that is described in more detail in [13].

Fig. 3: Stator surface with current density distribution and field strength in the air gap.
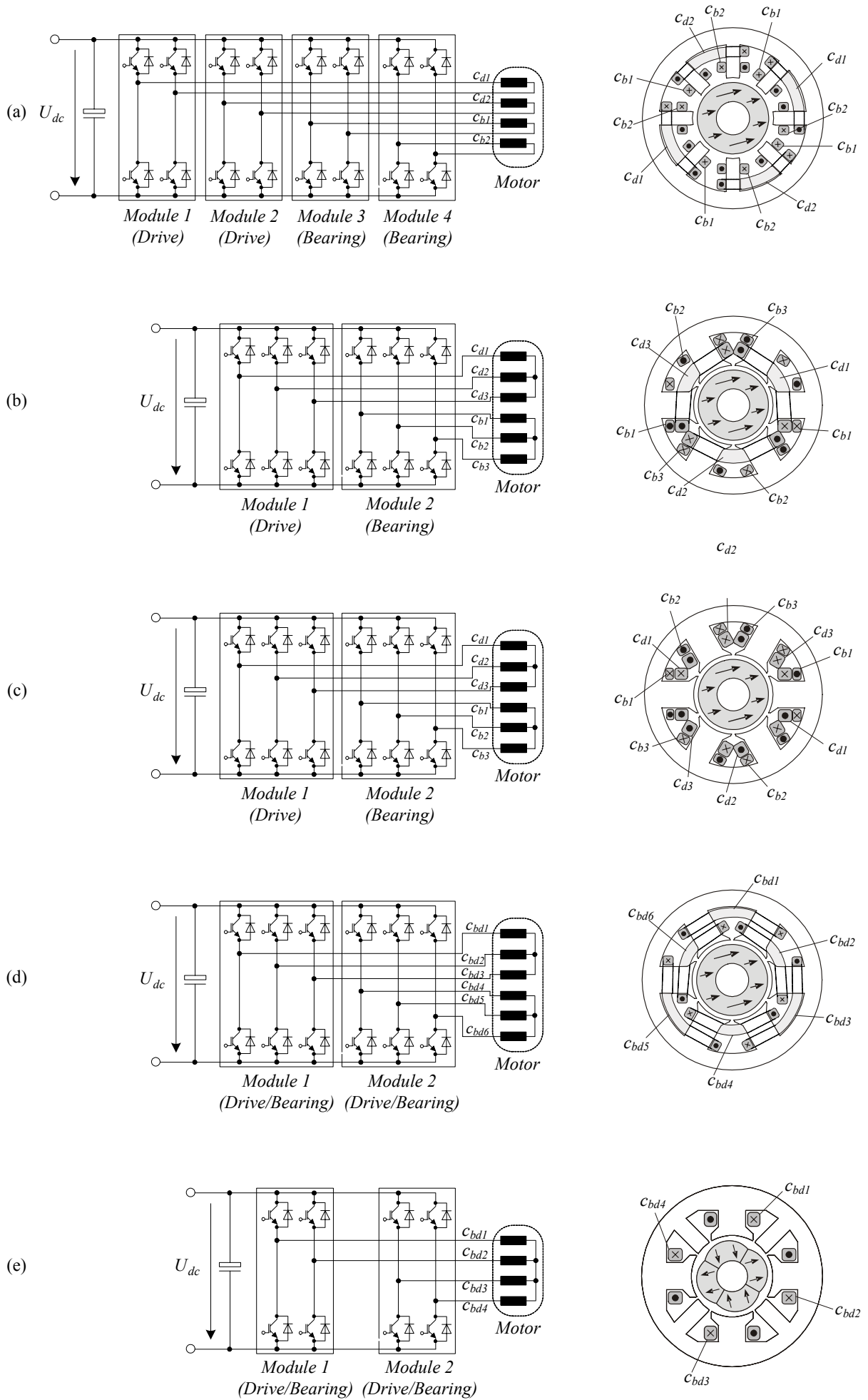
Fig. 4: Investigated BSM systems (a)-(e) consisting of the converter and the corresponding motor configuration.

III. INVESTIGATED BSM CONFIGURATIONS

With regard to the previously discussed performance indices different BSM configurations suitable for pump applications in general are assessed in the following. The targeted pump applications are specified by the maximum rotational speed, the rated torque and the maximum bearing force. As a base for the comparison the following assumptions are considered for the design of the BSM:

- The required rated drive power at the chosen operating point is $P_{DR} = 1200W$.
- The bearing system is designed in order to ensure the sufficient levitation forces for the whole operating range.
- The rotor diameter and the stator bore, respectively, are the same for all the chosen configurations.
- At rated torque, the current density in the windings is the same for all the chosen configurations.
- For all the presented configurations, the maximum allowable copper volume is chosen in order to reduce copper losses to the minimum.
- The flux density in the iron circuit is assumed the same for motor configurations (a)-(d). Furthermore, these configurations are realised as a temple motor whereas configuration (e) is from disc shape.

With these assumptions the assessment of the bearingless motors depicted in **Fig. 4** has been carried out. The configurations are the following:

- Fig. 4(a) shows a two-phase BSM with 12 separate windings for the drive and bearing system and a two-pole ($p = 1$) permanent magnet (PM) rotor. This symmetrical winding configuration represents the standard setup in today's bearingless pump systems [14] and possesses a total of eight claws. In order to independently generate the levitation forces and the motor torque eight full bridges are needed consisting of totally 16 power transistors. However, as has been shown in recent research [3], this motor embodiment can also be operated with only six half bridges. In order to ensure full control flexibility special modulation schemes must be employed [15]. For the here presented comparison the standard full bridge configuration will be used for sake of better comparability with the other concepts.

- Fig. 4(b) shows a three-phase BSM with nine separate windings and six claws for the drive and bearing systems and a two-pole ($p = 1$) PM rotor. In contrast to the motor configuration (a) the currents in the drive windings do not only generate the motor torque but also cause shear forces which then need to be compensated by the bearing currents and thus lead to higher losses. This drawback can be overcome with an adequate control algorithm presented in [16]. With this, the currents applied to the drive windings only lead to the generation of the desired torque without influencing the stable levitation of the impeller. The subsequent calculation of the copper losses for this motor embodiment is carried out with regard to this optimized control scheme.

- Fig. 4(c) shows a three-phase BSM with nine separate windings and six claws building the drive and bearing systems and a two-pole ($p = 1$) PM rotor. In this configuration, the drive currents do not lead to a generation of bearing forces as it is the case for the previously described configuration.

- Fig. 4(d) shows a three-phase BSM with six coils in total that generate the torque and the axial forces in common.

The current rating is the same for all coils and again, a two-pole ($p = 1$) PM rotor is employed. The pitch winding configuration results in a more efficient torque generation and results in lower power losses compared to the motor embodiments (a) - (c) as will be shown later on.

- Fig. 4(e) shows a four-phase BSM with four concentrated coils and a four-pole ($p = 2$) PM rotor. In contrary to the previously described configurations, which are realised in temple motor design with each claw being placed in an orthogonal manner to the back iron, this motor is realised in disc shape with a homogenously orientated lamination of the iron sheets. The absence of intersections between the claws and the back iron in this configuration has a major impact on the total iron losses as well be shown later on. Although the motor has four phases, the torque generation is equivalent to a single phase motor. This design is the simplest solution that allows a bearingless operation [16]. Furthermore, it offers the benefit that only four power half-bridges are needed to generate the torque and levitation currents in the motor.

The advantage of the converter topologies (b), (c), and (d) is that two intelligent three-phase power modules can be applied. On the one hand this leads to a significantly higher compactness. On the other hand the manufacturing cost is lowered, since such power modules are used in a large variety of applications and thus produced in high numbers. This is as well the case for full-bridge modules. However, their manufacturing quantities are lower since it is not common to operate three phase ac-motors with full-bridges as it is the case for three phase power modules.

As an immanent property of the motor embodiments shown in Fig. 4(d) and (e) the rated current of all windings are showing the same value which leads to a good utilization of the power electronics. On the other hand, the concentrated coils contribute to a coupled and highly nonlinear force and torque generation and thus require a more complex control algorithm in order to safely operate the motor. In contrary, for the configurations depicted in Fig. 4 (a)-(c) separate winding systems for force and torque generation are used. This results in different current ratings for the drive and bearing windings and hence leads to an unbalanced utilisation of the semiconductor devices if identical three-phase power modules are utilised. In order to quantify these facts a detailed comparison will be carried out in the following.

IV. POWER LOSSES

The evaluation of the losses in the motor and the power electronics are indispensable for a thorough comparison of the motor concepts. The most important portion is the copper losses occurring in the windings of the motor. In order to receive a better comparability between motors (a)-(e) the same current densities in the drive and bearing windings, respectively, have been assumed as design criteria for the calculation of the windings. A further important portion is the speed dependant iron losses, which are evaluated for all the presented embodiments subsequently. In section C the equations for the calculation of the switching and forward losses occurring in the power semiconductors are presented. With this, the total losses will be comparatively evaluated for the five concepts.

A. Copper losses

The calculation of the copper losses in the motor phases is given by the following equation:
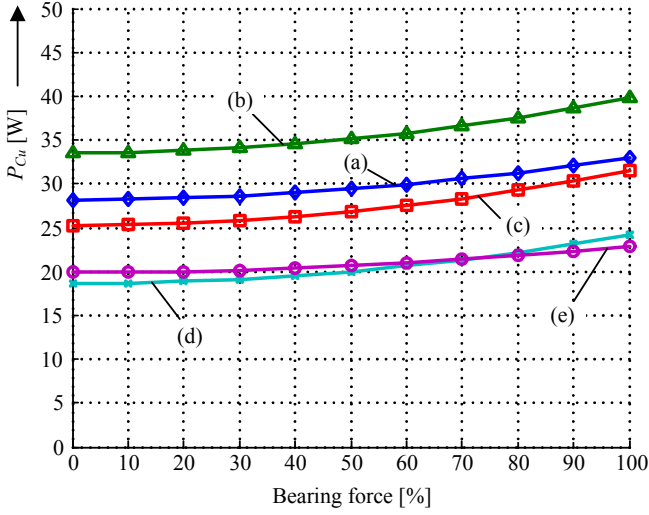
Fig. 5: Total copper losses subject to an increasing levitation force at the design point of 1200W drive power for the motor configurations (a)-(e) depicted in Fig. 4. 100% equals the maximum bearing force requested in a transient condition.

$$P_{Cu} = \sum_{i=1}^{m} R_i \cdot I_{i,rms}^2, \tag{6}$$

with m as the number of winding phases of the subjected motor and R_i as the corresponding resistance value, which is calculated with

$$R_i = \frac{\rho_{Cu} \cdot l_w}{A_{Cu}}. \tag{7}$$

Here, l_w stands for the average winding length of the drive or bearing winding, ρ_{Cu} the specific resistance of copper, and A_{Cu} the wire cross area.

Doing this for all of the motor embodiments presented in Fig. 4 for the load point specified in section III leads to a loss distribution as depicted in **Fig. 5**. Looking at the values at zero bearing force reveals that motor embodiment (d) only generates 56% of the losses occurring in configuration (b). While increasing the bearing force up to 100% (which equals 20N) this proportion stays almost the same. The largest increase in losses due to the generation of the levitation forces arises for motor (d). There, at maximum force the losses are increased by 30% compared to the load point with no currents in the bearing phases.

B. Iron losses

According to [17], the hysteresis losses of iron can be approximated under the assumption that the magnitude of the flux density $\hat{B}$ of an alternating field is in the range of 0.2-1.5T by the following equation:

$$P_{Hy} = c_{Hy} \cdot f_e \cdot \hat{B}^{1.6} \cdot m_{Fe}. \tag{8}$$

The hysteresis losses are thus linearly dependant on a material constant c_{Hy}, the electrical frequency f_e of the motor, and the iron mass m_{Fe}, while the dependency on the flux density is of higher order. On the other hand, the eddy current losses [18] in the stator iron are given by

$$P_{Ed} = c_{Ed} \cdot f_e^2 \cdot \hat{B}^2 \cdot d_{Fe}^2 \cdot m_{Fe}, \tag{9}$$

if the iron circuit is built up with isolated laminated sheets with a thickness of d_{Fe}.

However, for the evaluation of the hysteresis and eddy current losses the magnetic flux density in the iron path can not be assumed to have a homogeneous distribution, wherefore (8) and (9) can not be used directly. In order to calculate the iron losses accurately, the whole stator needs to be segmented into k parts with each having a constant flux density $\hat{B}_i$ and a mass $m_{Fe,i}$. The whole iron losses of each motor configuration can then be calculated according to

$$P_{Fe} = P_{Hy} + P_{Ed} =$$
$$= m_{Fe,i} \cdot \left(c_{Hy} \cdot f_e \cdot \sum_i^k \hat{B}_i^{1.6} + c_{Ed} \cdot f_e^2 \cdot \sum_i^k \hat{B}_i^2 \cdot d_{Fe}^2 \right). \tag{10}$$

This correlation can also be written as

$$P_{Fe} = k_1 \cdot n_e + k_2 \cdot n_e^2 \tag{11}$$

with k_1 being the linear and k_2 being the square loss factor, respectively and the motor speed n. These factors, which have been extracted from simulations and validated by measurements on experimental test setups, are compiled in Table I for all configurations.

TABLE I: IRON LOSS FACTORS

Configuration	(a)	(b),(c),(d)	(e)
k_1 [W/1000 rpm]	0.921	0.850	0.671
k_2 [W/(1000 rpm)^2]	0.645	0.602	0.153

It can be seen that especially the square loss factor (due to the eddy current losses) is significantly lower for configuration (e). The main reason is the fully radial construction of that setup with an equally oriented lamination of the iron sheets. In contrary, the concepts (a)-(d) are built in temple motor design, where the stator parts have to be linked in an orthogonal manner and a continuous lamination is not possible. Furthermore, setup (e) has a lower iron mass, which is, however, compensated by the higher electrical frequency (due to $p = 2$).

In total, as shown in Fig. 6, a clear advantage for the motor configuration (e) is given regarding the iron losses, especially for higher rotational speeds. However, due to dynamical limitations (as will be discussed later), this concept does not allow rotational speeds above 8000 rpm, which is a limiting factor for some applications.

C. Power Electronics losses

All of the presented motor configurations are operated with a
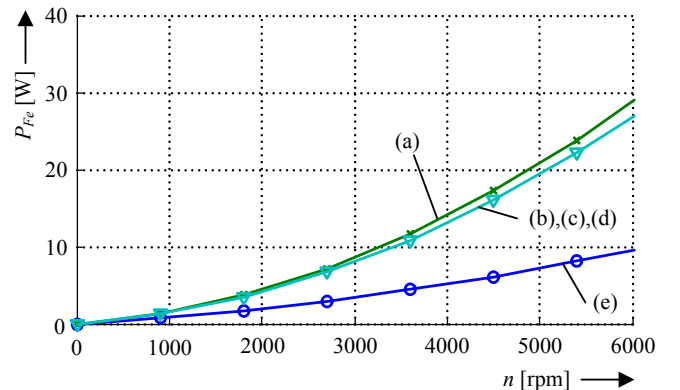
Fig. 6: Total iron losses P_{Fe} of the presented motor configurations (a)-(e) in dependence of the motor speed n.

symmetrical PWM switching pattern. Due to this and the utilization of similar components in the drive and bearing system of all configurations the switching losses can be evaluated based on the same switching loss energy data. The switching losses of a device are then given by integration of the loss energy over a $\pi/2$-wide interval.

$$P_{Sw} = f_s \cdot \frac{2}{\pi} \int_0^{\pi/2} w(i) d\varphi. \tag{12}$$

With the assumption of a linear dependency of the loss energy on the switched current

$$w(i) = k_i \cdot i \tag{13}$$

for a given voltage the calculation of the switching losses based on the component specific factors k_{on}, k_{off} and k_{rev} for the turn-on, the turn-off and the reverse recovery losses, respectively, can be utilised. These parameters, which have been evaluated by switching loss measurements on a three phase power module [19] account to $k_{on,} = 22.54\mu J/A$, $k_{off} = 11.43\mu J/A$ and $k_{rev} = 1.35\mu J/A$ for a dc-link voltage of $U_{dc} = 325V$. For the sake of a fair comparison these parameters have also been used for the full-bridge topology (cf. Fig. 4(a), two-phase configuration) and the half-bridge topology (cf. Fig. 4(e), four-phase configuration). With this, the total switching losses per bridge leg are given by

$$P_{PE,Sw} = \frac{2 \cdot f_s}{\pi} \cdot (k_{on} + k_{off} + k_{rr}) \cdot \hat{I}. \tag{14}$$

The forward characteristics of the semiconductors can be approximated by a forward voltage drop and a forward resistance. The parameters $U_{CE,0}$ and r_{CE} for the IGBT, and $U_{F,0}$, r_F for the diode, respectively, have also been evaluated by measurements and account to $U_{CE,0} = 1.11V$, $r_{CE} = 77m\Omega$, $U_{F,0} = 1.05V$ and $r_F = 83m\Omega$. With this, the conduction losses of any semiconductor can be derived by

$$P_{Fw,T} = U_{CE,0} \cdot I_{T,avg} + r_{CE,on} \cdot I_{T,rms}^2 \tag{15}$$

$$P_{Fw,D} = U_{F,0} \cdot I_{D,avg} + r_F \cdot I_{D,rms}^2 \tag{16}$$

The total power electronics losses in the half-bridges due to the bearing and drive currents can then be evaluated.
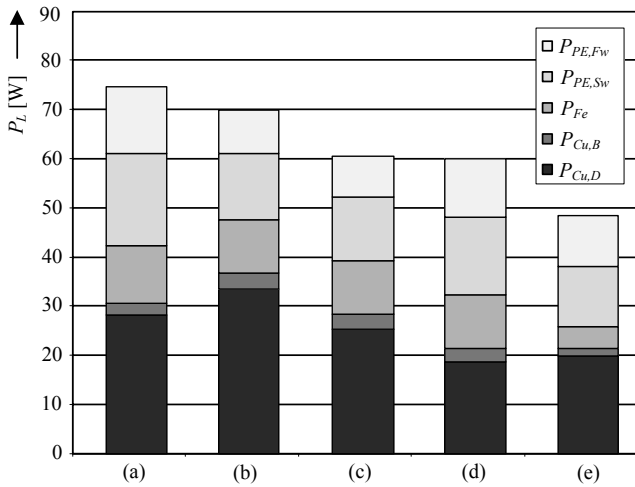
Fig. 7: Overall loss distribution for the motor and converter configurations depicted in Fig. 4(a)-(e). The shown losses are the copper losses in the drive system ($P_{Cu,D}$) and in the bearing system ($P_{Cu,B}$), the iron losses (P_{Fe}), the switching losses ($P_{PE,Sw}$) and the forward losses ($P_{PE,Fw}$) in the power electronics.

D. Total losses

With the help of the before-presented equations the overall losses P_L including the copper, the iron and the power electronics losses can be calculated. Their distribution is depicted in Fig. 7.

This comparison has been carried out for a rated drive power of $P_{DR} = 1200W$ at 70% bearing force at a speed of $n = 3600rpm$, which is a typical operating point value. It can be seen that the total losses are lowest for configuration (e), followed by setup (d).

V. POWER ELECTRONICS REQUIREMENTS

Another important figure for the evaluation of the motor topologies is their Volt-Ampere (VA) power electronics requirement. In the past, a lot of research has been carried out on the VA requirements of different motors [20], [21]. Among different definitions the VA rating in terms of inverter peak voltage and rms current of the motor is the most suitable for the comparison of the evaluated BSM topologies.

The VA rating in a mathematical form is given by

$$P_{VA} = \sum_{i=1}^m \hat{U}_i \cdot I_{i,rms}, \tag{17}$$

with the rms current $I_{i,rms}$ and the peak phase voltage $\hat{U}_i$. When neglecting the resistive voltage drop across the drive or bearing winding the required value of the peak phase voltage $\hat{U}_i$ results in

$$\hat{U}_i = \sqrt{\left(\omega L_i \hat{I}_i\right)^2 + \hat{U}_{i,ind}^2}, \tag{18}$$

with the phase inductance L_i, the peak phase current $\hat{I}_i$ and the amplitude of the induced voltage $\hat{U}_{i,ind}$.

For the configurations (a)-(c), which feature separated drive and bearing systems, different peak phase voltage requirements can be calculated for both systems. However, due to the availability of only one common dc-link voltage of the converter, the higher voltage requirement (which occurs for the drive system) has been considered for both systems. Hence, the bearing system has a broad stability margin to compensate for external disturbances. For the configurations (d)-(e), which generate the levitation forces and the torque in the same windings, a certain stability margin for the bearing system has to be added explicitly in order to also guarantee a safe operation. Measurements on laboratory prototypes have shown that the voltage requirement has to be increased by a factor of 1.3 for the considered speed range, which is already taken into account for this comparative evaluation. For higher rotational speeds this margin would have to be increased even more and it was observed experimentally that for a dc-link voltage of 325V the configurations (d) and (e) cannot be operated above 8000rpm anymore. Additionally, for configuration (e) the maximum achievable speed is also limited by the digital control, which has to deal twice the electrical frequency due to $p = 2$ as compared to the other topologies.

The VA requirements scaled to the rated mechanical power are depicted in Fig. 8 for the different motor designs. One can see that the required bearing forces have significant impact on the VA requirement of the motor. This is especially the case for motor (d), where at 100% bearing force, which equals 20N, the VA requirement is nearly doubled as compared to zero force. If only the drive system is taken into
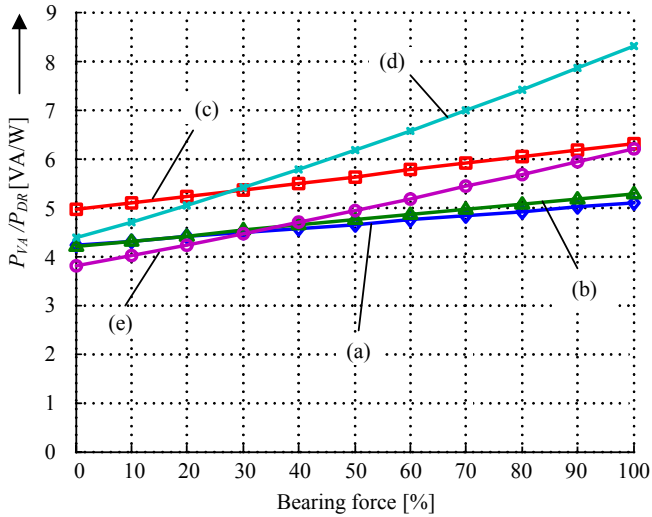
Fig. 8: Normalised VA requirement of the presented motor configurations (normalisation basis: rated drive power P_{DR} = 1200W).

account (0% bearing force), configuration (e) demands the lowest VA requirement.

However, this condition does not arise in normal operation of a BSM since levitation forces are always needed in order to safely operate the system. For the considered operating point with 70% bearing forces, which is a typical value for pump applications, motor configurations (a) and (b) are the most efficient solutions regarding the necessary VA requirement of the converter.

VI. COST RELATED FACTORS

As mentioned in the beginning, BSM pump systems are getting more and more targeted for applications, where mass production becomes feasible. Therefore, additional cost-related factors must be taken into consideration for a complete comparison. In Table II a qualitative comparison of the concepts is given for these factors in addition to the previously discussed performance indices (power losses and VA requirement).

TABLE II
QUALITATIVE COMPARISON OF THE DIFFERENT BSM CONCEPTS

Motor	(a)	(b)	(c)	(d)	(e)
Power losses	−	−	✓	✓	+
VA requirement	+	+	✓	−	✓
Copper/Iron mass	−	−	−	−	+
Realisation effort	✓	✓	✓	✓	+
Control complexity	+	+	+	−	−
Scalability	+	+	+	−	−

As has been shown in section IV, configurations (d) and (e) are the favourable ones, if only the losses in the motor and the power electronics are considered. At the chosen operating point the overall losses occurring in configuration (e) are 65% of those resulting in configuration (a).

In terms of VA requirements, the motor setups (a) and (b) have been found to be preferable for applications, where significant bearing forces occur, e.g. for pumps. On the other hand, configuration (d) has the highest VA requirements and therefore leads to the largest power electronics volume.

The comparison of the copper and iron mass, which is re-

quired to realise the different motor embodiments, is lowest for configuration (e). The radial design of the iron circuit, which does not need additional vertical claws, as they are required in the temple motor configurations (a)-(d), results in an iron mass which is almost half as compared to the other concepts.

Looking at the embodiments from a manufacturing perspective and with this considering the necessary realisation effort reveals motor (e) as the most promising solution. This mainly emerges from the disc shape structure of this configuration, which offers certain production advantages. First, the four identical coils can directly be wound on the stator claws in one step, which simplifies the manufacturability. In addition, the iron circuit can be realised with a horizontally laminated iron stack. Due to the absence of additional vertical claws the manufacturing effort is clearly reduced compared to the temple motor configurations (a)-(d). Finally, the disc shape setup also offers the possibility of integrating the power electronics part in the motor while still keeping the thereby resulting total case volume in the range of the temple motor configurations without integrated power electronics. In addition, this greatly reduces the cabling effort. However, the sensor concept of motor (e) for the position detection of the impeller is the most difficult of all the presented configurations due to the shape of the iron circuit and the limited space that is available for the insertion of the sensors. Its design also influences the design of the pump impeller in terms of hydraulic efficiency. This fact also strongly influences the applicability of this concept in high pressure/flow applications. However, taking all the before-mentioned issues into account, the realization effort clearly is the lowest for configuration (e).

The control complexity of the presented motor embodiments highly depends on the chosen winding configuration. The fact that the currents, which are generating torque and levitation forces, are applied to the same coils in common for configurations (d) and (e), results in a more sophisticated control structure as it is the case for configurations (a)-(c). In the latter, the control of the drive and bearing system can be done independently. This results in a less complex control structure as for motors (d) and (e).

As explained in section V, the scalability of the motor configurations towards higher speeds and pressure is best for configurations (a)-(c). This results from the independent drive and bearing system, where due to the utilisation of the same dc-link voltage the bearing system usually features a large dynamical voltage margin to compensate for external disturbances. In contrast, for configurations (d) and (e) the stability margin for the bearing system has to be added explicitly in order to guarantee a safe operation. This voltage margin together with the maximum available dc-link voltage is the limiting factor for the maximum achievable drive speed for these concepts. In today's semiconductor applications a strong demand arises for pumps with high pressure ratings. For these applications motor configurations (d) and (e) cannot be considered as suitable solutions due to their limited speed capability.

Summing up, it can be stated that configuration (e) is highly interesting for future cost-sensitive bearingless motor applications such as pumps for plating industry, mixers for biotechnology processes, or heat and cooling pumps. However, the applicability of this configuration is limited to the low/medium speed range and is therefore not suitable for high-pressure applications. In this area, configuration (a) still seems to be the most preferable solution.

VII. Summary

In this paper two-, three- and four- phase bearingless slice motors (BSM) have been comparatively discussed based on performance indices in order to find the most suitable motor embodiment for more cost sensitive application areas of next generation bearingless pump systems. The comparison has been carried out for a typical pump operating point (rated mechanical drive power 1200W, bearing forces in the range of 0-20N) and the performance indices have been defined as the occurring power losses in the converter and the motor, the power electronics VA requirements in order to achieve the operating point and cost related manufacturing issues (such as copper and iron masses, realisation effort in consideration of mass production, control complexity, and scalability towards higher speed and pressure ranges).

The comparison has not revealed a clear superior concept in all aspects, but has given a better insight to the specific attributes and possibilities of each concept. Generally, it can be stated that the three-phase motor configurations (b)-(d) do not show a clear advantage in none of the considered aspects, wherefore they will barely be selected as the next generation bearingless motor concept.

On the other hand, the four-phase motor configuration (e) seems to be a promising concept for future cost-sensitive applications in the low pressure and low/medium speed range, e.g. pumps for plating industry, mixers for biotechnology processes, or heat and cooling pumps. The advantages of this concept in terms of small iron and copper masses and easy manufacturability are mainly arising from its radial construction. In addition, the compact design allows the integration of the power electronics in the motor housing with a resulting volume comparable to that of the temple motor design without integrated electronics.

However, for high pressure applications in upcoming semiconductor applications, where speeds above 8000rpm are demanded, this concept cannot be considered anymore due to its inherent speed limitations. There, the standard two-phase topology (a) is still the most preferable solution due to the independent drive and bearing winding system.

VIII. References

[1] M. Neff, N. Barletta, R. Schöb, "Magnetically levitated centrifugal pump for highly pure and aggressive chemicals", *PCIM Conference* 2000, June 6-8, 2000, Nuremberg, Germany.

[2] R. Schöb, N. Barletta, J. Hahn, "The Bearingless centrifugal pump – A perfect example of a mechatronics system", *1st IFAC-Conference on Mechatronic Systems*, Darmstadt, Germany, 18-20 September 2000.

[3] M.T. Bartholet, T. Nussbaumer, P. Dirnberger, J.W. Kolar, "Novel converter concept for bearingless slice motor systems", IEEE Industry Applications Conference 2006, *Conference Record of the 41st IAS Annual Meeting*, October 2006, Tampa, USA, vol. 5, pp. 2496-2502.

[4] A. Chiba, R. Furuichi, Y. Aikawa, K. Shimada, Y. Takamoto and T. Fukao, "Stable operation of induction-type bearingless motors under loaded conditions", *IEEE Trans. Ind. Appl.*, vol. 33, no. 4, pp. 919-924, Jul./Aug. 1997.

[5] M. Ohsawa S. Mori and T. Satoh "Study of the induction type bearingless motor", *Proc. 7th Int. Symp. Magnetic Bearings*, Zurich, Switzerland, Aug. 2000, pp. 389-394.

[6] A. Chiba, T. Deido, T. Fukao and M.A.Rahman, "An analysis of bearingless AC motors", *IEEE Trans. Energy Convers.*, vol. 9, no. 1, pp.61-67, Mar. 1 94.

[7] W. K. S. Khoo, R. L. Fittro and S. D. Garvey, "AC polyphase self-bearing motors with a bridge configured winding", *Proc. 8th Int. Symp. Magnetic Bearings*, Mito, Japan, Aug. 2002, pp. 47-52.

[8] Y. Okada, K. Dejima and T. Ohishi, "Analysis and comparison of PM synchronous motor and induction motor type magnetic bearings", *IEEE Trans. Ind. Appl.*, vol. 31, no. 5, pp. 1047-1053, Sep./Oct. 1995.

[9] Y. Okada, S. Myamoto and T. Ohishi, "Levitation and torque control of internal permanent magnet type bearingless motor", *IEEE Trans. Contr. Syst. Technol.*, vol. 4, no. 5, pp. 565-571, Sep. 1996.

[10] S. Silber, W. Amrhein, P. Bosch, R. Schob, N. Barletta, „Design aspects of bearingless slice motors", *IEEE Trans on Mechatronics*, vol 10, pp. 611-617, Dec. 2005.

[11] Maxwell® 3D distributed by Ansoft Corporation, http://www.ansoft.com.

[12] K. Simonyi, Theoretische Elektrotechnik, Leipzig, Germany: Barth Verlagsgesellschaft GmbH, 1993.

[13] D. Schröder, Elektrische Antriebe – Grundlagen, 2. Auflage, Springer, 2000.

[14] Levitronix Pumps: http://www.levitronix.com.

[15] M.T. Bartholet, T. Nussbaumer, D. Krähenbühl, F. Zürcher, J.W. Kolar, „Modulation concepts for the control of a two-phase bearingless slice motor utilizing three-phase power modules", *IEEE Power conversion conference 2007*, Nagoya, Japan, 2007.

[16] S. Silber, "Beiträge zum lagerlosen Einphasenmotor, Dissertation, Johannes Kepler Universität, Linz, 2000.

[17] C. P. Steinmetz, "On the law of hysteresis", *Proc. IEEE*, vol. 72, pp. 196-221, Feb. 1984.

[18] C. Heck, "Magnetische Werkstoffe und ihre technische Anwendung, Dr. Alfred Hüthig, Heidelberg, 2. Auflage, 1975.

[19] International Rectifier: Integrated Power Hybrid IC for Appliance Motor Drive Applications, IRAM136-3063B, Preliminary Datasheet DR-2 (2007).

[20] M. Barnes, Ch. Pollock, "Power electronic converters for switched reluctance drives", *IEEE Trans. on Power Electron.*, vol. 13, pp. 1100-1111, Nov. 1998.

[21] T.J.E. Miller, "Switched Reluctance Motors and Their Control", Oxford, U.K: Magna Physics/Clarendon, 1993.